Supplementary Information

Towards bubble-free, centimeter-sized bilayer graphene enabled by backside lamination

Mingzhi Yan[1,2†], Xin Gao[2,3,4†], Jun Qian[2,3†], Xiaoyin Gao[3], Jilin Tang[2,3,4], Yuechen Wang[2,3,4], Yani Wang[2,3], Junchuan Tang[3], Liming Zheng[3], Kaicheng Jia[2], Fei Jia[1], Hongtao Liu[3*], Guanghui Gao[1,2*], Hailin Peng[2,3,4*]

[1]*School of Chemical Engineering & Advanced Institute of Materials Science, Changchun University of Technology, Changchun 130012, P.R China.*

[2]*Beijing Graphene Institute, Beijing 100095, P. R. China.*

[3]*Center for Nanochemistry, Beijing Science and Engineering Center for Nanocarbons, Beijing National Laboratory for Molecular Sciences, College of Chemistry and Molecular Engineering, Peking University, Beijing 100871, P. R. China.*

[4]*Academy for Advanced Interdisciplinary Studies, Peking University, Beijing 100871, P. R. China.*

[†]These authors contributed equally to this work.

[*]Corresponding author. E-mail: hlpeng@pku.edu.cn, ghgao@ccut.edu.cn, htliu-cnc@pku.edu.cn

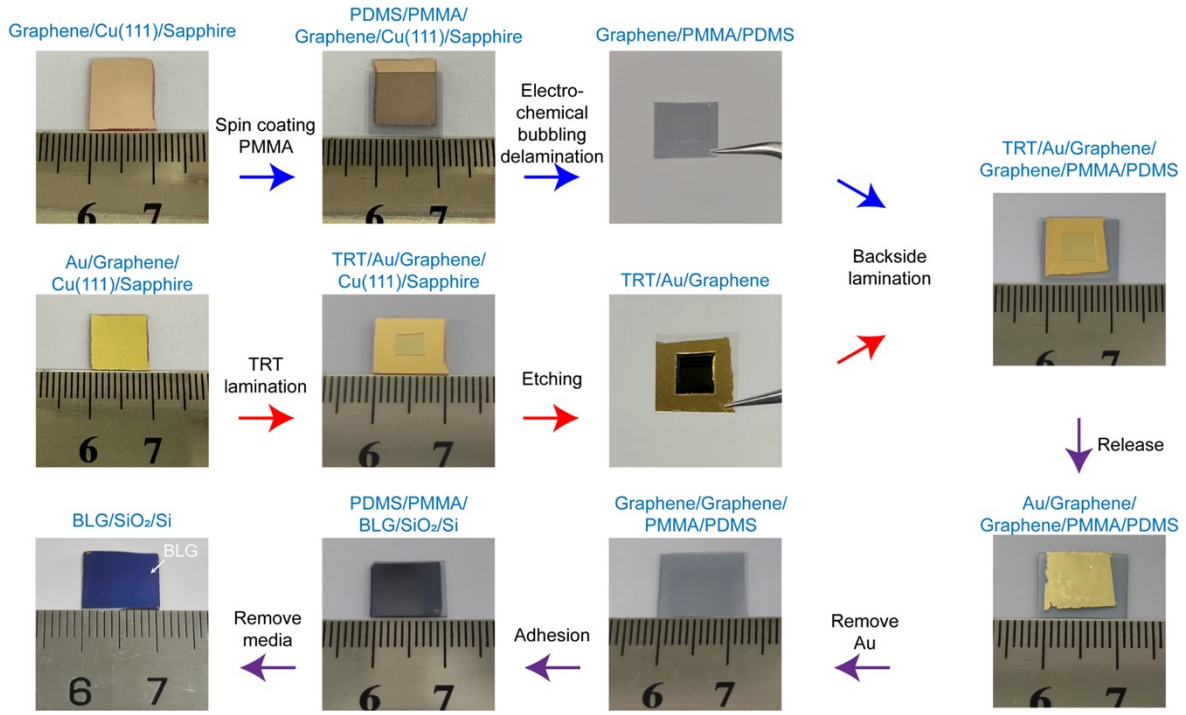

Fig. S1 Step-by-step protocol of BSL method for fabricating bilayer graphene (BLG).

1. First, the graphene wafer was cut into two pieces. Two different kinds of transfer mediums were deposited on graphene. A ~50 nm thermally evaporated gold film and another ~50 nm sputtered gold film were sequentially deposited on one piece of graphene, and then TRT was attached to obtain the TRT/gold/graphene/Cu(111)/sapphire composite structure. The other piece of graphene was spin-coated with PMMA, and laminated with PDMS obtaining the PDMS/PMMA/graphene/growth substrate composite structure.

2.The TRT/gold/graphene film was detached from the growth substrate by etching the Cu film in an aqueous solution of 1 mol L^{-1} $(NH)_4S_2O_8$. The PDMS/PMMA/graphene film was exfoliated from growth substrate by electrochemical bubbling method. Rinsed with deionized water, and the composite films were fully dried in atmosphere.

3.The two fresh and clean graphene backside surfaces were laminated with each other in air at 80 °C within 5 min to obtain a bubble-free interface.

4. TRT was released at 130 ℃, and gold film was removed by electrochemical bubbling in 1 mol L^{-1} NaOH aqueous solution. After rinsing with deionized water to remove residual etchant, the composite film was fully dried in atmosphere.

5. The PDMS was exfoliated at 180 °C, and the PMMA/BLG/SiO_2/Si was baked at 180 °C for 2 h. Finally, the PMMA was removed with the vapor of hot acetone, leaving the twisted bilayer graphene

on the target substrate.

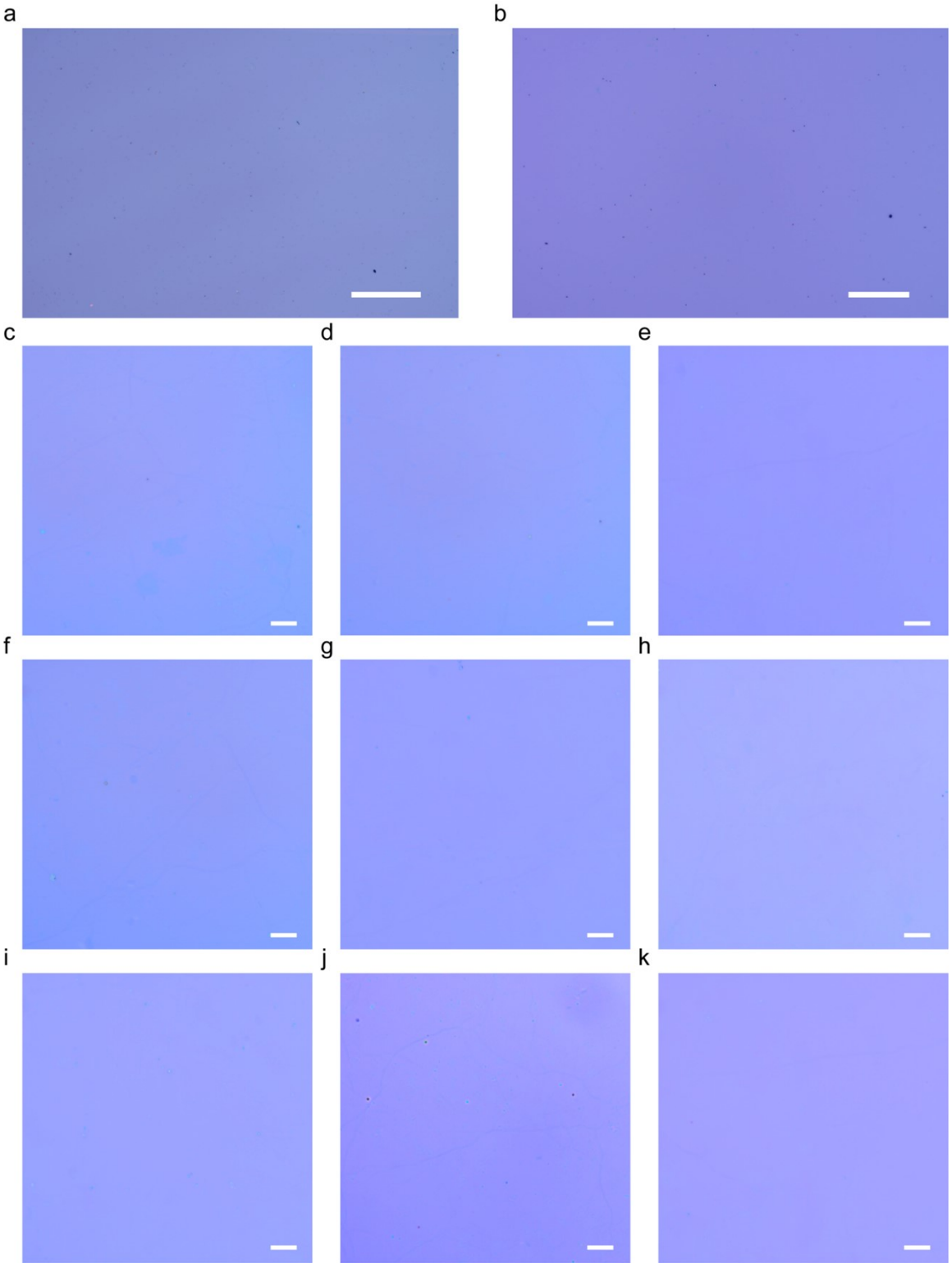

Fig. S2 Optical microscopy images of bilayer graphene transferred by BSL method. (a) Optical microscopy image of bilayer graphene transferred by BSL method with a 5× objective lens. The scale bar is 500 μm. (b) Optical microscopy image of bilayer graphene transferred by BSL method with a 20× objective lens. The scale bar is 100 μm. (c–k) Optical microscopy images of bilayer graphene

transferred by BSL method with a 100× objective lens. All the scale bars are 10 μm.

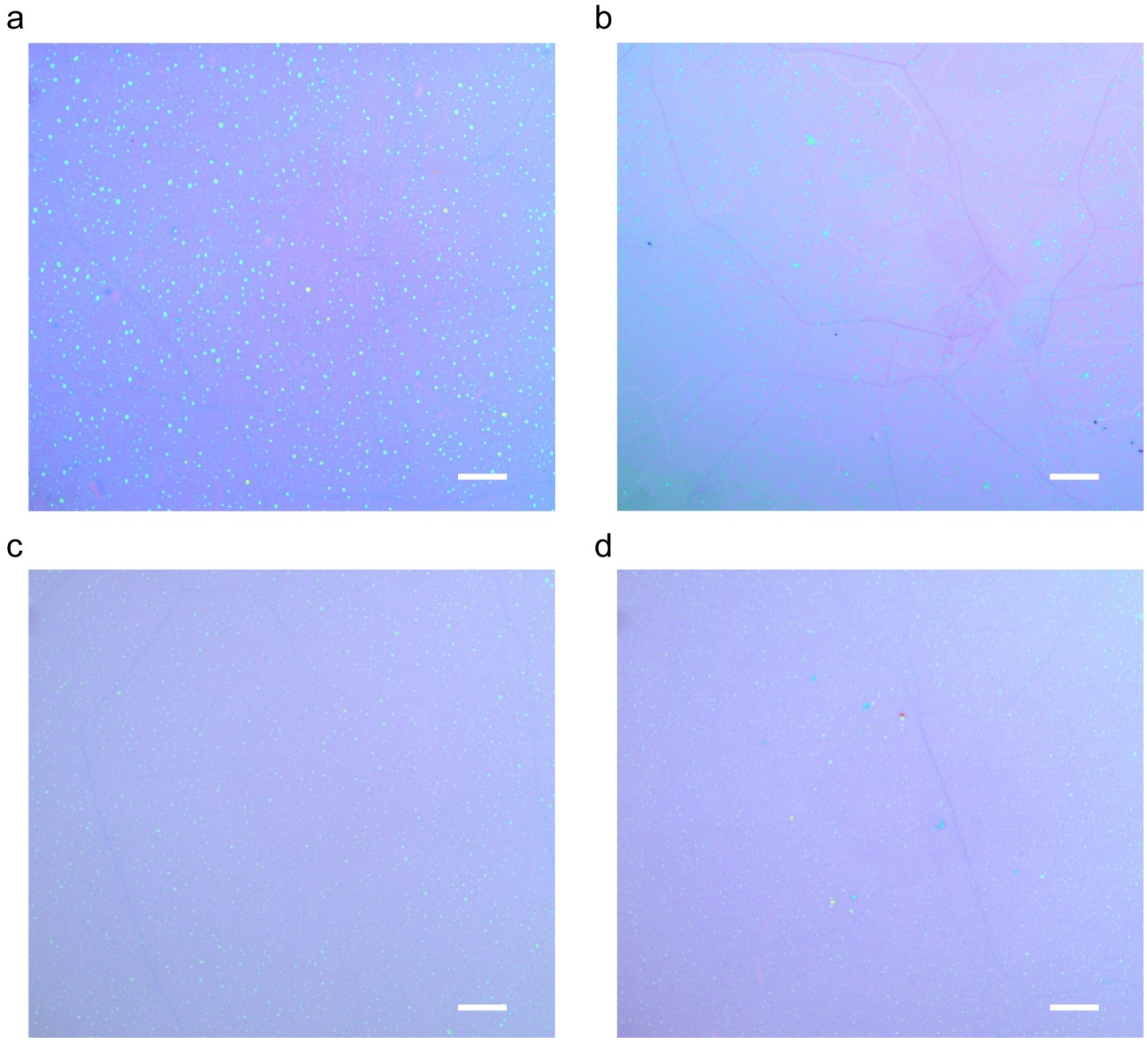

Fig. S3 Optical microscopy images of bilayer graphene transferred by LBL method. (a–d) Optical microscopy images of bilayer graphene transferred by LBL method with a 100× objective lens. All the scale bars are 10 μm.

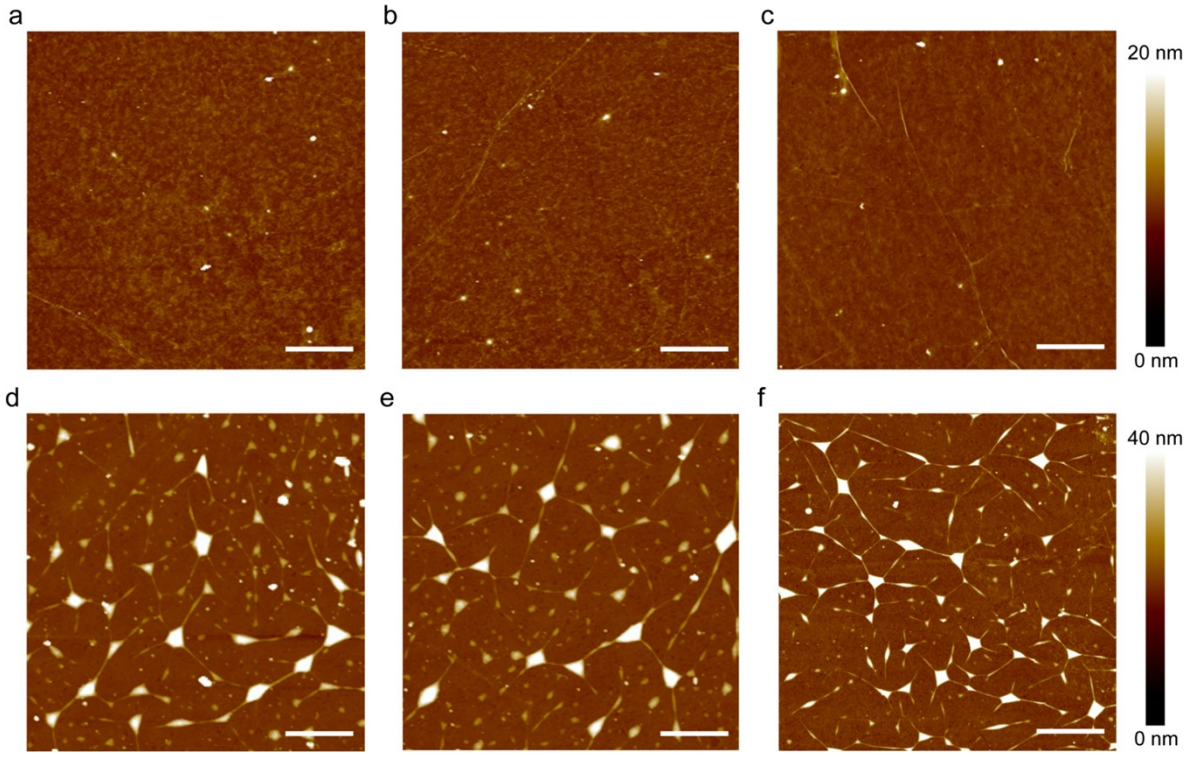

Fig. S4 Typical AFM images of BSL- and LBL-transferred bilayer graphene. (a–c) Typical AFM images of bilayer graphene transferred by BSL method. (d–f) Typical AFM images of bilayer graphene transferred by LBL method. All the scale bars are 1 μm.

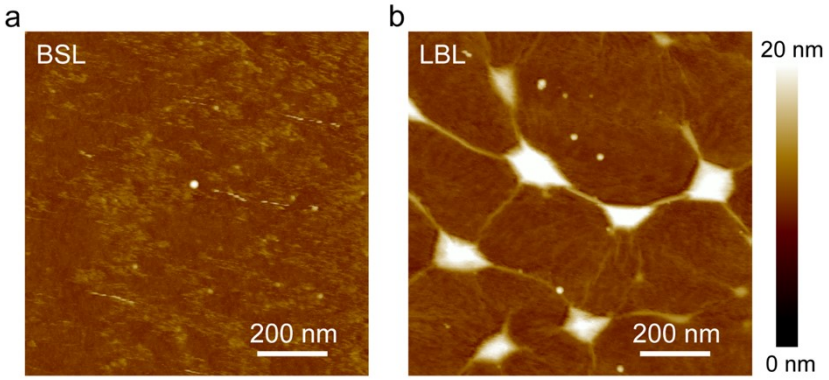

Fig. S5 High-resolution AFM images of BSL- and LBL-transferred bilayer graphene. (a) Typical AFM image of BSL-transferred bilayer graphene. (b) Typical AFM image of LBL-transferred bilayer graphene.

To confirm the absence of nano-bubbles in BSL-transferred bilayer graphene, high-resolution AFM images were conducted. The BSL-transferred bilayer graphene shows a nano-bubble-free morphology, while LBL-transferred graphene has lots of nano-bubbles and sub-micro-bubbles.

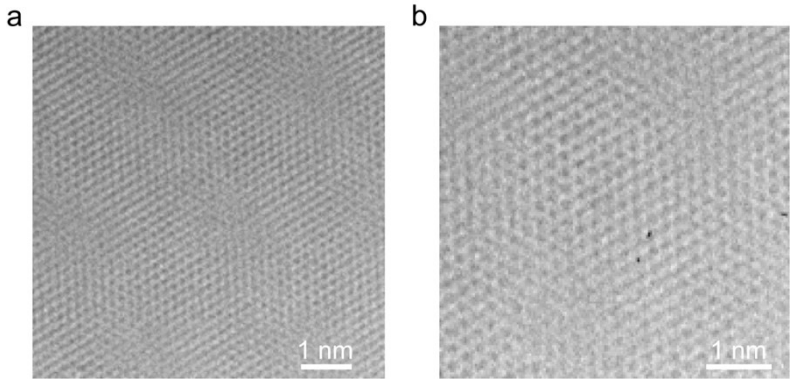

Fig. S6 High-resolution TEM images of BSL-transferred bilayer graphene. (a) Copy of the inset of Fig. 2b. (b) TEM image of BSL-transferred graphene with a larger magnification.

The nano-bubble of contamination can be identified by high-resolution TEM (HRTEM)[1,2]. HRTEM images were collected to confirm the absence of nano-scale interfacial bubble. The clear moiré pattern of BSL-transferred bilayer graphene indicates the clean and bubble-free interface.

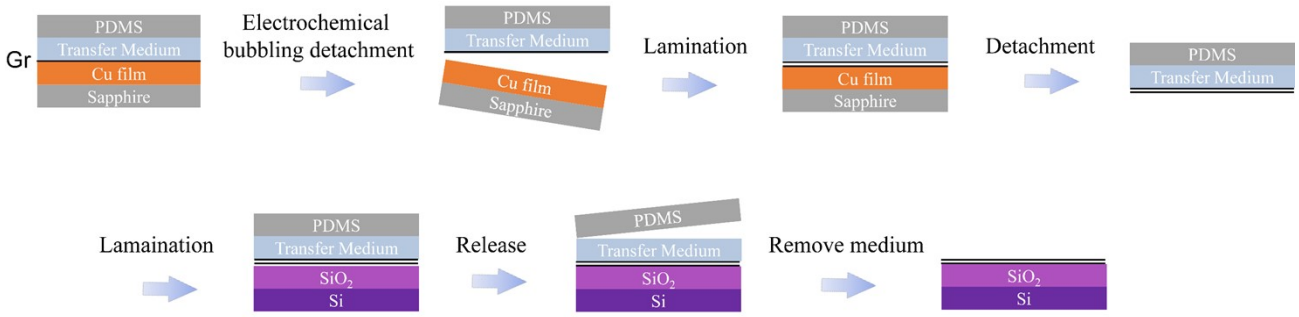

Fig. S7 Schematic illustration of bilayer graphene stacked by LBL method.

The layer-by-layer transfer method can avoid interface contacting with polymer. However, amorphous carbon and post-adsorbed contaminant may be trapped at the interface.

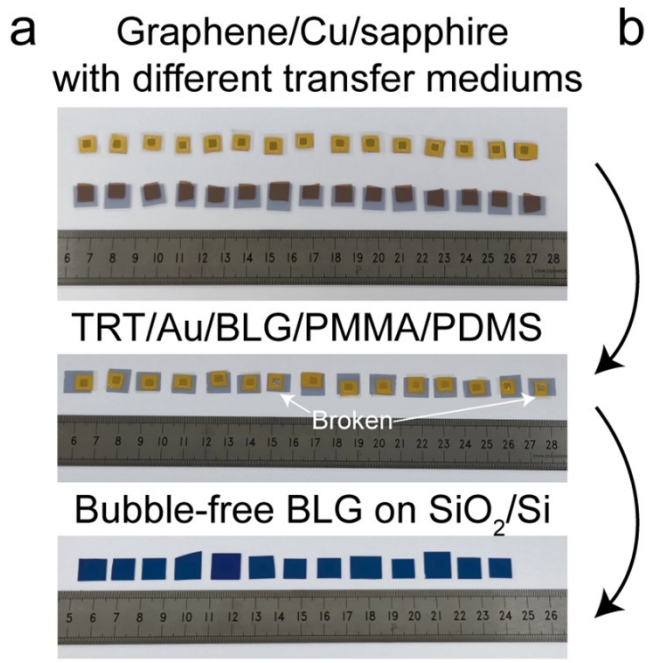

b

	Batch 1	Batch 2
Total	15	10
Broken	2	1
Intact	13	9
Yield	88%	

Fig. S8 Reproducibility and yield of the BSL method. (a) 15 BSL-transferred bilayer graphene in one batch. (b) The statistic of yield of bilayer graphene obtained via the BSL method.

25 BSL-transferred bilayer graphene were fabricated in two batches, and the batch one samples are shown in Fig. S8a. As shown in Fig. S8b, the BSL method was highly reproducible with a yield of ~90%.

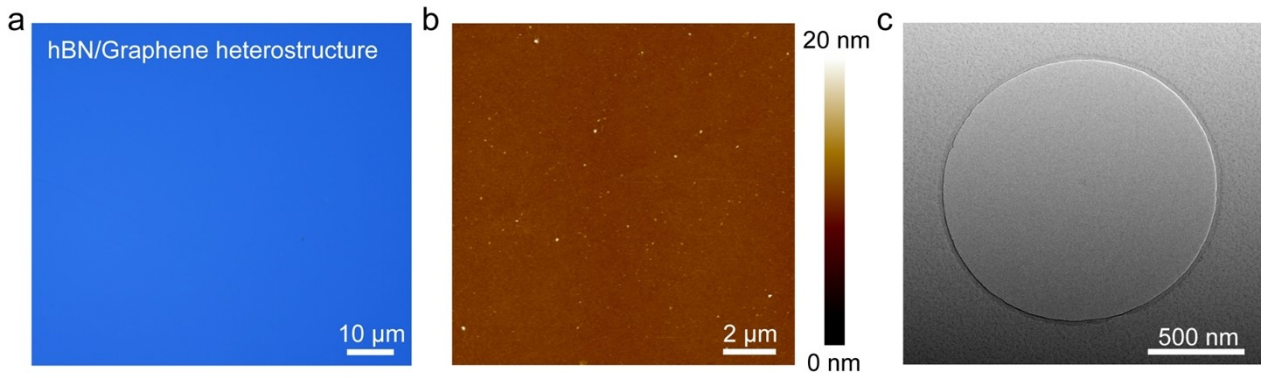

Fig. S9 Bubble-free CVD hBN/graphene heterostructure fabricated by BSL method. (a–c) OM image (a), AFM image (b) and TEM image (c) of BSL-transferred hBN/graphene heterostructure.

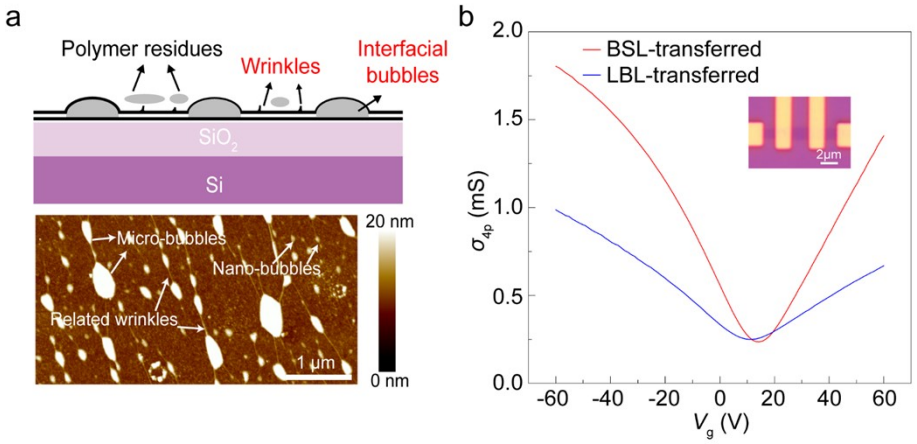

Fig. S10 Analysis of electrical performance of BSL- and LBL-transferred bilayer graphene. (a) Scattering factors affecting the carrier mobility of transferred bilayer graphene. (b) Typical transfer characteristics of field-effect transistors (FETs) fabricated from BSL- and LBL-transferred bilayer graphene. The inset presents an optical microscopy image of the FET device.

As shown in Fig. S10a, both micro- and nano-bubbles, as well as wrinkles and creases connecting the bubbles, will act as scattering centers, which would degrade the electrical performance of graphene. Therefore, we have fabricated field-effect transistors (FETs) based on BSL- and LBL-transferred bilayer graphene to study the electrical properties of the bilayer graphene (Fig. S10b). The carrier mobility of BSL-transferred bilayer graphene (~6,800 $cm^2\ V^{-1}\ s^{-1}$) is much larger than that of LBL-transferred bilayer graphene (~2,800 $cm^2\ V^{-1}\ s^{-1}$), indicating that fewer scattering centers exist in BSL-transferred graphene. Note that the p-doping of both BSL- and LBL-transferred bilayer graphene may be caused by the polymer residues on the surface. The charge carrier mobility μ was extracted from linear fit of the conductivity σ using the following equation (1):

$$\mu_{4p} = \left(\frac{L}{WC_{ox}\Delta V}\right)\left(\frac{dI_{ds}}{dV_g}\right) \quad (1)$$

where C_{ox} is the gate capacitance (1.15×10^{-8} F cm^{-2} for 300 nm thick SiO_2); L and W are the spacing between the voltage probes and channel width, respectively; I_{ds} is the drain-to-source current; ΔV is the voltage drop between the two probes separated by L; and V_g is the back-gate voltage[3].

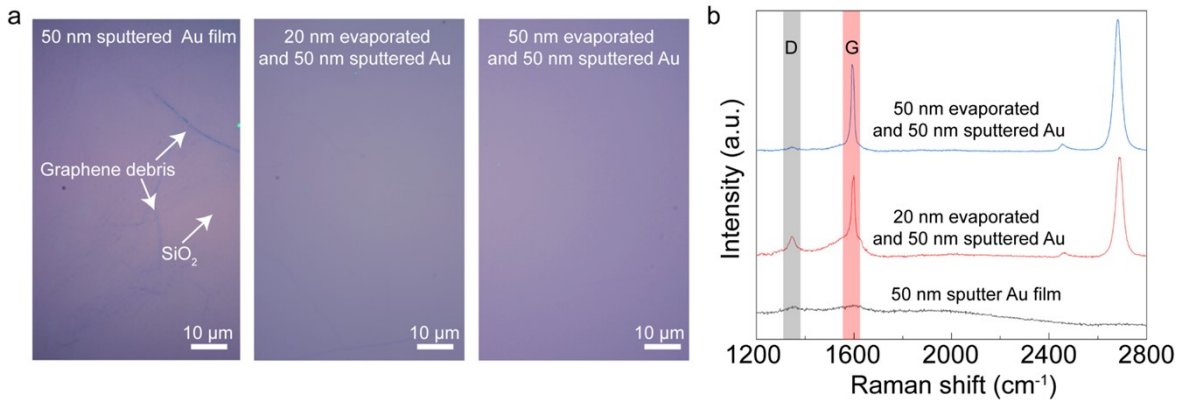

Fig. S11 Monolayer graphene transferred on SiO_2/Si with Au films deposited by different methods (a) Optical microscopy images of the monolayer graphene on SiO_2/Si substrates. (b) Raman spectra of the graphene. Grey and red columns indicate the D peak and G peak of graphene, respectively.

A ~50 nm thermally evaporated Au film was first deposited to protect graphene from damage, and another ~50 nm sputtered Au film was deposited to ensure the mechanical strength of Au film and reduce the time of deposition, the latter of which will damage the graphene film by the high energy atomic clusters. As shown in Fig. S11, the monolayer graphene transferred with thermally evaporated 50 nm and sputtered 50 nm Au film shows an intact morphology and a Raman spectrum with a negligible D peak. However, graphene transferred with only sputtered 50 nm Au films was almost completely damaged leaving only graphene debris, and the thin evaporated Au film (~20 nm) cannot protect graphene completely, leading to a large D peak.

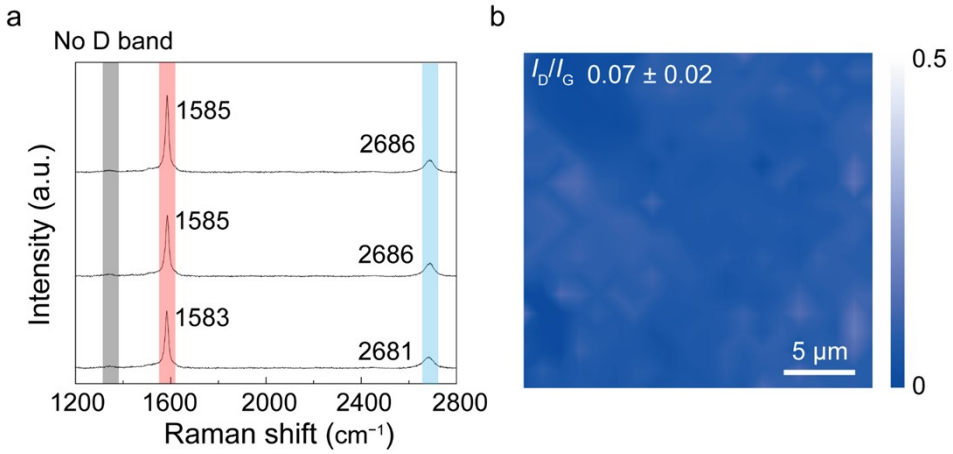

Fig. S12 Defect analysis of bilayer graphene transferred by BSL method. (a**)** Raman spectra of bilayer graphene transferred by BSL method. **(**b**)** Spatial Raman map of I_D/I_G.

The intensity ratio of the D-peak to the G-peak (I_D/I_G) is usually used as an important parameter to characterize the density of graphene defects. The I_D/I_G ratio of BSL-transferred bilayer graphene is 0.07 ± 0.2, showing a relative low defect density. According to the relationship between the ratio and defect density (n_D):

$$n_D(\mathrm{cm}^{-2}) = (7.3 \pm 2.2) \times 10^9 \times E_L^4 \times (I_D/I_G) \quad (2)$$

where E_L is the laser excitation energy of the Raman system[4].

The defect density of BSL-transferred bilayer graphene is about 1.5×10^{10} cm^{-2}.

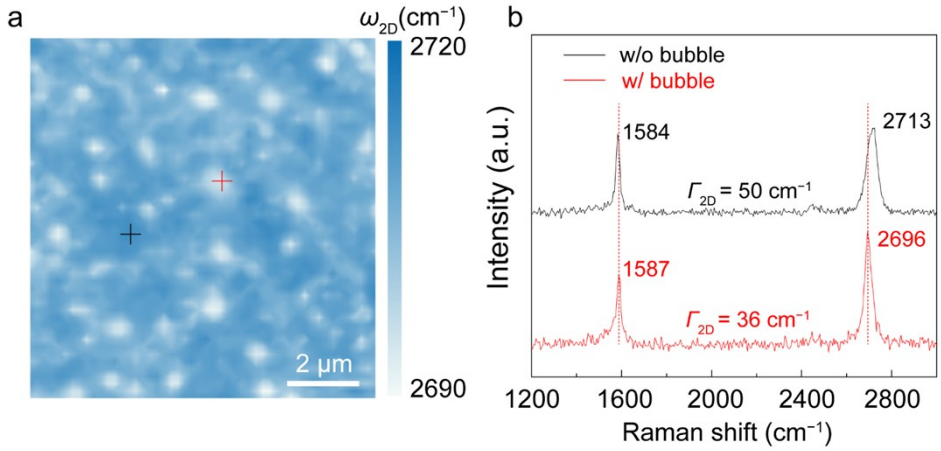

Fig. S13 Comparison of Raman spectra of bilayer graphene with and without interface bubbles. **(**a**)** Spatial 2D-peak's position maps of bilayer graphene with bubbles obtained by LBL transfer method. The red cross indicates the area with interface bubble, and the black cross indicates the bubble-free area. **(**b**)** Raman spectra of the points marked with red and black crosses in (a). The red line corresponds to the location of the red cross, and the black line corresponds to the black cross.

Two Raman spectra were extracted from the spatial Raman map of LBL-transferred bilayer graphene, one with interface bubble and another without bubble as shown in Fig. S13a. The interface bubble will introduce tensile stress in graphene and causes red-shift of 2D peak's position. In addition, the interface contamination increases the distance between graphene layers and reduces the interlayer coupling, leading to a smaller 2D peak's FWHM. In comparison, the Raman spectrum of bilayer graphene without bubble shows similar peaks with AB-stacked bilayer graphene, which indicates the improved interlayer coupling in bubble-free bilayer graphene (Fig. S13b).

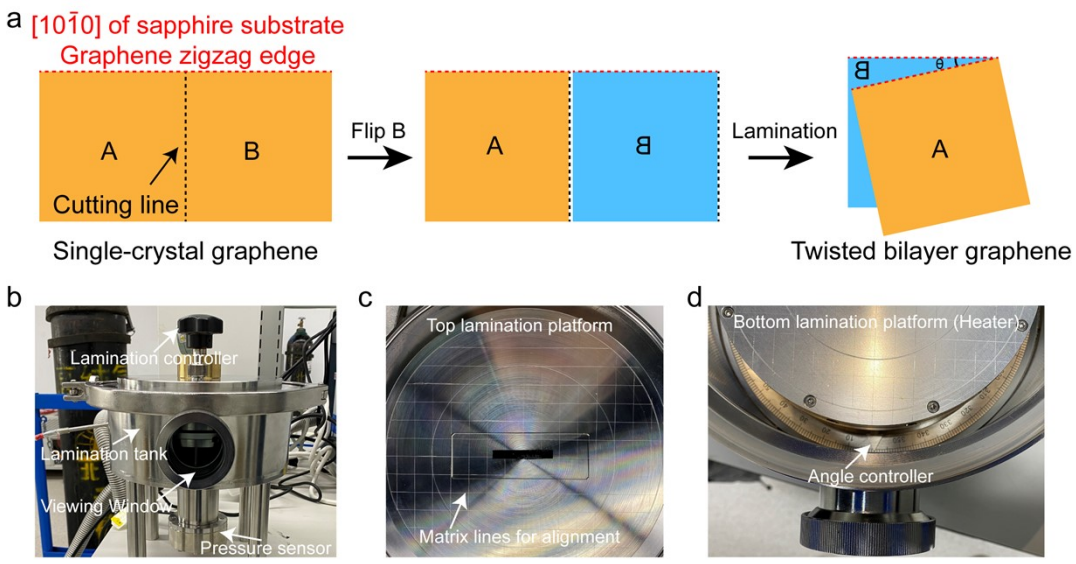

Fig. S14 Determination of twist angle of transferred bilayer graphene. (a) Scheme of the twist angle control method. (b–d) The home-made alignment equipment for angle control.

The twist angle of bilayer graphene is predetermined by edge of graphene/Cu(111)/sapphire wafers, which is the [10$\bar{1}$0] crystal orientation of sapphire substrate corresponding to the graphene zigzag edge. As shown in Fig. S14a, one single-crystal graphene/Cu/sapphire is cut into two pieces, and the twist angle can be determined by the graphene zigzag edge. The angles ranging from 0° to 360° can be controlled by a home-made alignment equipment with an accuracy of 1° (Fig. S14b–d). The exact twist angle is confirmed by measuring the angle between the two sets diffraction spots in the SAED images.

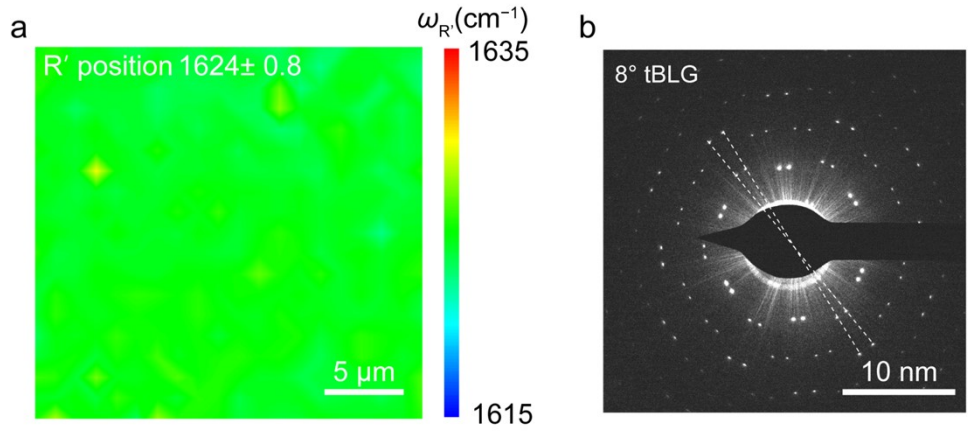

Fig. S15 Raman spectrum and SAED characterization of 8° tBLG. (a**)** Raman mapping of $\omega_{R'}$. **(**b**)** Typical SAED pattern of 8° tBLG.

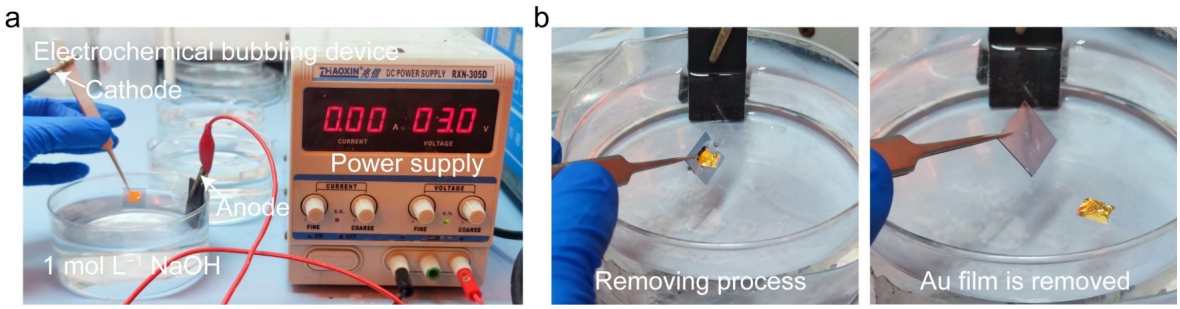

Fig. S16 Electrochemical bubbling method for Au film delamination. (a) Electrochemical bubbling device. (b) Au film delamination process.

The method is similar to the conventional electrochemical bubbling method. As shown in Fig. S16, 1 mol L^{-1} NaOH was used as electrolyte, and graphite plate and the Au film were act as the anode and cathode, respectively. Constant and low voltage (2–3 V) was applied and small H_2 bubbles generated at both the surface of Au film and the interface between Au film and graphene, enabling the delamination of Au film.

Reference

1 S. J. Haigh, A. Gholinia, R. Jalil, S. Romani, L. Britnell, D. C. Elias, K. S. Novoselov, L. A. Ponomarenko, A. K. Geim & R. Gorbachev, *Nat. Mater.*, **2012**, 11, 764–767.

2 A. V. Kretinin, Y. Cao, J. S. Tu, G. L. Yu, R. Jalil, K. S. Novoselov, S. J. Haigh, A. Gholinia, A. Mishchenko, M. Lozada, T. Georgiou, C. R. Woods, F. Withers, P. Blake, G. Eda, A. Wirsig, C. Hucho, K. Watanabe, T. Taniguchi, A. K. Geim, and R. V. Gorbachev, *Nano Lett.,* **2014**, 14, 3270–3276.

3 Daowei He, Jingsi Qiao, Linglong Zhang, Junya Wang, Tu Lan, Jun Qian, Yun Li, Yi Shi, Yang Chai, Wei Lan, Luis K. Ono, Yabing Qi, Jian-Bin Xu, Wei Ji, Xinran Wang, *Sci. Adv.,* **2017**, 3, e1701186.

4 L. G. Cançado, A. Jorio, E. H. M. Ferreira, F. Stavale, C. A. Achete, R. B. Capaz, M. V. O. Moutinho, A. Lombardo, T. S. Kulmala and A. C. Ferrari, *Nano Lett.,* **2011**, 11, 3190–3196.